Online at: https://researchtrendsjournal.com ISSN No: 2584-282X

INTERNATIONAL JOURNAL OF TRENDS IN EMERGING RESEARCH AND DEVELOPMENT

Volume 2; Issue 1; 2024; Page No. 133-139

Received: 07-12-2023
Accepted: 16-02-2024

Importance and growing neural network for autonomous detection and classification of brain tumor

[1]Mrutyunjaya and [2]Dr. Manish Saxena

[1]Research Scholar, Department of Computer Science, Himalayan University, Arunachal Pradesh, India
[2]Assistant Professor, Department of Computer Science, Himalayan University, Arunachal Pradesh, India

DOI: https://doi.org/10.5281/zenodo.12794693

Corresponding Author: Mrutyunjaya

Abstract

In this study, we tackled the complex task of detecting brain tumors in MRI scans using a large dataset of brain tumor images. We found that fine-tuning a cutting-edge YOLOv7 model through transfer learning significantly enhanced its ability to detect gliomas, meningiomas, and pituitary tumors. Our deep learning model demonstrated promising results by accurately pinpointing the presence and exact location of brain tumors in MRI scans. Our approach achieved superior accuracy compared to conventional methods, achieving an impressive 99.5% accuracy in our evaluations. However, we recognize the need for further investigation and validation to ensure the efficacy of our method in detecting small tumors. The challenge of identifying small tumors underscores the ongoing necessity for research in brain tumor detection and continual improvement of our detection systems. By pursuing this path, we strive to advance diagnostic capabilities for both patients and medical professionals in the demanding fight against brain cancers.

Keywords: Brain tumor, MRI, YOLOv7 model, MRI

Introduction

The Central Nervous System (CNS), comprising the brain and spinal cord, manages numerous biological functions such as coordination, analysis, decision-making, command issuance, and integration. The human brain is immensely complex due to its intricate physical structure. Conditions affecting the CNS, like strokes, infections, brain tumors, and migraines, pose significant challenges in terms of diagnosis, assessment, and effective treatment development. Brain tumors, arising from abnormal growth of brain cells, particularly perplex neuropathologists and radiologists in early detection via Magnetic Resonance Imaging (MRI), a challenging and error-prone manual process. These tumors manifest as masses caused by aberrant nerve cell development. There are approximately 130 different types of brain and CNS tumors, ranging from benign to malignant, and from uncommon to prevalent occurrences. Malignancies can either originate within the brain (primary brain tumors) or spread there from elsewhere in the body (secondary or metastatic brain tumors). Primary brain tumors develop from brain cells or can be enclosed within the nerve cells surrounding the brain. They exhibit diverse characteristics, encompassing both benign and malignant forms. On the other hand, secondary brain tumors, also termed metastatic brain tumors, represent the most common type of malignant brain tumors. Notably, while benign tumors typically do not metastasize to other body areas, secondary brain tumors are invariably cancerous and pose a grave health threat.

A unique LPDF-RVM and GCNN for automatic BT segmentation are presented in this paper. First, MR brain scans are obtained for input. In addition, the wiener filter-based noise removal technique and picture normalization are carried out in tandem with the skull stripping procedure. The extraction of HOG features and the Gray-Level Co-Occurrence Matrix (GLCM) are then carried out. LPDF-RVM is used as a segmentation technique based on the features, and GCNN is applied after. A thorough study of the simulation was done to show how much better the model that was provided performed.

The recently discovered technology preprocesses the input image before segmenting it. First, the input MRI is normalized, and then additional processing is performed.

The Wiener Filter (WF) is used to quantify the unclear images and remove noise. Next, in order to avoid the skull in MRI images and labeling models, skull stripping is done. Following ROI identification, GLCM and HOG are used to process feature extraction. The retrieved features are used to inform the use of GCNN for classification. LPDF-RVM is used as a method of segmentation. The newly deployed approach's flow diagram is shown in Fig-1.

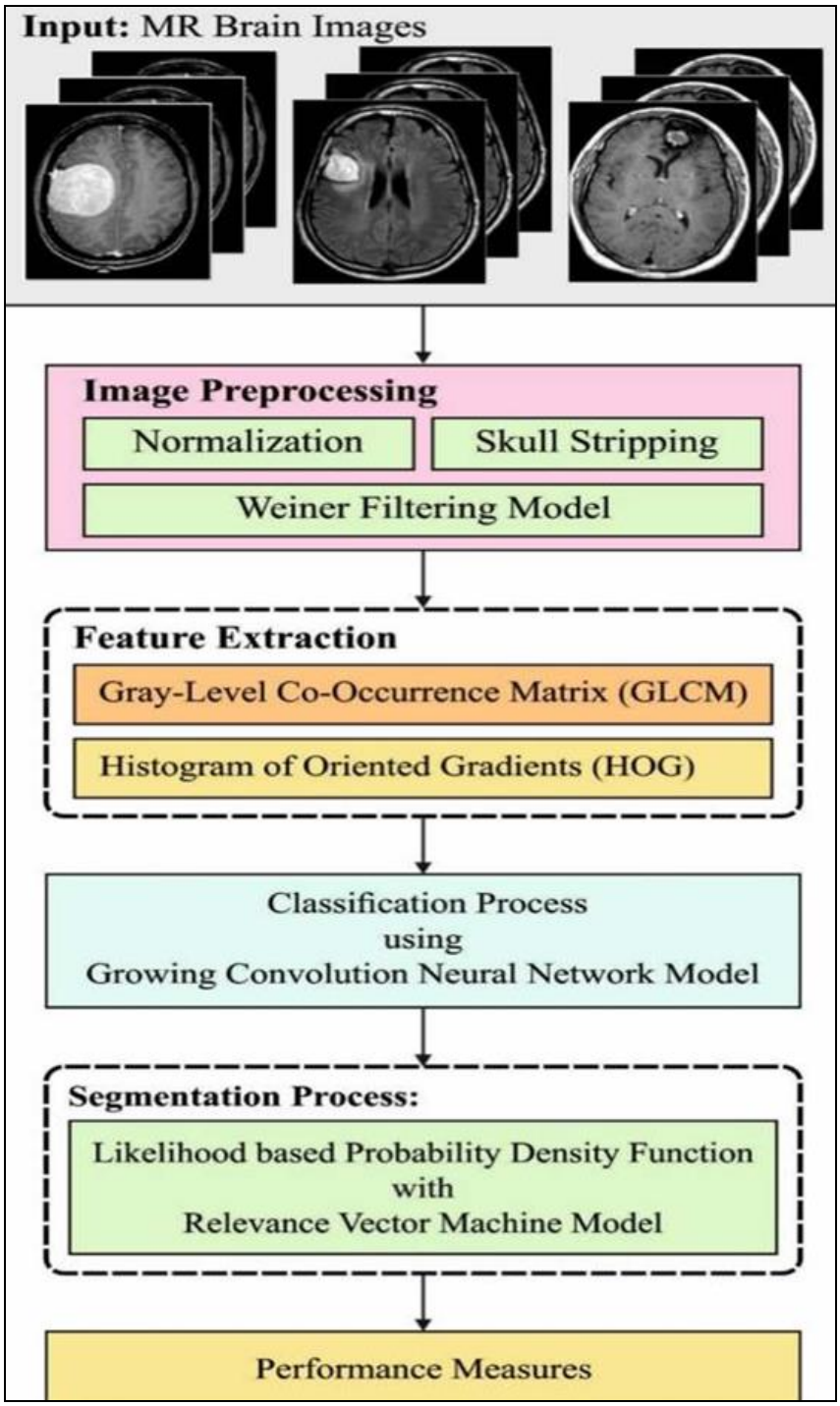

Fig 1: Working process of proposed model

Preprocessing

Here, the input image is preprocessed in order to remove noise and uncertainty before performing additional operations. There have been three steps taken in the preliminary stage. Normalization is done first, then noise is removed using WF, and finally, skull stripping is handled. The procedure of separating the brain's surrounding tissue from the brain itself is known as "skull stripping."

Feature Extraction

In the newly developed approach, specific features are extracted from the preprocessed images namely,

- GLCM
- HOG

Gray-level co-occurrence matrix (GLCM)

Texture is a key consideration in this feature for creating

meaningful visual representation. The definition of the GLCM feature extraction model is a matrix form that contains the incidence of frequency and angular orientation (θ) of two pixels with distinct intensities at a distance d from each other inside the image. Additionally, processing of the GLCM feature extraction is done in four angle directions: 0°, 45°, 90°, and 135°. In order to distinguish between things, texture analysis takes into account the grayscale properties of each object.

Contrast
It gives the intensity contrast value between a pixel and its neighbor in an image. Consequently, contrast is defined as:

$$Co = \sum \sum (i - j) 2p(i, j)$$

Where p(i, j) implies the GLCM matrix.

Correlation
It is a value of measuring the pixel correlation to the neighbor of an image that is written as:

$$Correlation = \sum_i \sum_j \frac{ijp_d(i,j) - \mu_x \mu_y}{\sigma_x \sigma_y})$$

Where the symbols μx, μy, and σx, σy stand for the probability matrix GLCM's mean and standard deviation (SD) with respect to both row-wise x and column-wise y.
Energy
The sum of squared units in GLCM is also named uniformity. Energy is illustrated as:

$$Energy = \sum_i \sum_j p^2(i,j)$$

Homogeneity
In GLCM, homogeneity refers to how closely distributed the elements are. Similar to the grayness values, which may be explained as follows, the homogeneity value is maximal in photographs.

$$Homogeneity = \sum_i \sum_j \frac{p(i,j)}{1 + |i - j|})$$

Histogram of oriented gradients (HOG)
A feature descriptor used in CV techniques is known as the HOG. Next, objects are extracted from applied photos using HOG. It measures the gradients of intensity to determine the form and representation of an item. The main idea of HOG is that the distribution of intensity gradients in a picture indicates the form and shape of nearby objects. As a result, the image is divided into tiny, interconnected areas called cells, each of which has induced HOG pixels. Descriptor is called composite of histograms after that. Local histograms can be contrast-normalized for improved accuracy by analyzing the intensity across large-scale images, which is then utilized to normalize the cells.
a) Gradient Computation: HOG features are classifying the image window as tiny spatial regions named cells for a cell collecting local 1-D histogram of gradient directions across the pixels. Particularly, the model requires extraction of information from an image for the filter kernels.

$[-1, 0, 1]$ *and* $[-1, 0, 1]$

Gradient sampling is approximated using several discrete derivative masks and Gaussian smoothing.
b) Orientation Binning: The cell histograms are generated based on the HOG features when a computation is finished. Based on the orientation of the gradient element, a pixel estimates a weighted vote to the edge orientation histogram channel. The votes are then gathered within the orientation bins throughout small spatial regions known as cells.

c) Descriptor Block: In a gradient, local normalization of efficiency necessitates the collection of cells as massively scaled, spatially connected blocks. The HOG descriptor is essentially a vector plus a subset of each block region's normalized cell histograms. Blocks that overlap, therefore, indicate an excess cell contribution and are compared to the final descriptor. Rectangular R-HOG blocks and circular C-HOG blocks are the two main blocks used.

d) Block Normalization: There are four different models of block normalization in this module. Using the block histograms as a guide, consider V as a non-normalized vector. Then, the normalization factor is represented as indicated in the as follows:

$$L2 - norm \quad f \frac{v}{\sqrt{||v||_2^2 + e^2}}$$

L2-norm and clipping (reducing the high values of v to 0.2) and renormalizing are illustrated by,

$$L1 - norm \quad f = \frac{v}{||v||_{1+e}}$$

$$L1 - sqrt \quad f = \sqrt{\frac{v}{||v||_{1+e}}}$$

Growing convolution neural network (GCNN)
Following feature extraction, GCNN classification is carried out. It limits the amount of parameters for the system with complex applications, improves the forthcoming function, and activates the encoding features from inputs. Using generic characteristics, GCNN was trained to do a variety of tasks without requiring any modifications to the way the input was organized. On the other hand, the capacity of the network to dynamically expand while adhering to rules distinguishes NN from GCNN. First, it is necessary to describe how many layers-such as CONV, RELU, and POOL-there are. After that, the system grew on its own in an interactive manner, and Back propagation (BP) was available on both fixed edges and nodes of different layers. The feedback procedure for collective filters will be used by BP to train the network until it reaches the predetermined

accuracy threshold. When a system is completely wrong, the network focuses on the fewest possible edges. As a result, the error confluence speed is adjusted to a minimum threshold value and the training process is expanded for the growing algorithm. Eventually, the GCNN system creates the network architecture in a dynamic manner after being overworked before segmentation is begun.

Segmentation

The process of segmenting the image into its infected and non-infected portions is finally completed. Segmentation is carried out with the use of LPDF-RVM. The original RVM's sparsity-based working function is calculated using picture smoothness. Consequently, the lack of a clear prior structure throughout the weight variance indicates that the choice of kernel functions and parameters determines the sparsity. Consequently, problems with overfitting and underfitting have surfaced. To solve the issue, the LPDF-RVM technique has been used. Additionally, the greatest likelihood function is used to determine the ideal hyperparameters and assigns 0 to the weights depending on those hyperparameters in order to ensure the model's sparsity. For instance, the RVM scheme is depicted as follows for a sample set ($x1$, $x2$.,..,), where yi ∈ {+1, −1} denotes the sample's class label:

$$y(x) = \sum_{n1}^{N} w_n K(x, x_n) + w_0$$

Where K(,) defines the kernel function and wn implies the weight of samples. In addition, RVM applies a Bernoulli distribution for developing PDFs:

$$p(t_i|x) = N(t_i|y(x_i; w), \sigma^2)$$

Where the desired value is p($ti|x$) as well as the variance is $\sigma 2$.

To eliminate overfitting, the newly developed model is applied and illustrated as:

$$p(x_i|\mu) = \prod_{i=1}^{N} p(x_i|\mu) = (2\pi\sigma^2)^{-\frac{n}{2}} exp\,(-\frac{1}{2\sigma^2}\sum_{i=1}^{n}(x_i - \mu)^2)$$

Whereas the normal distribution is indicated by μ, the function ($xi|\mu$) is used to indicate the location where the density is dependent on the unknown parameter.

It is not possible to evaluate the posterior probability of weights once the classification procedure is put into practice. Consequently, Laplacian theory is used to approximate the estimation: find the potential weight wMP for recently developed α.

$$log\{p(t|w)\ P(x_i|\mu)\} = \sum_{n=1}^{N}[t_n log y_n + (1 - t_n)log(1 - y_n)] - \frac{1}{2}w^T \mu w$$

Where,

yn = {(xn; w)}

The log posterior probability is normalized in the Laplacian model.

$$\nabla_w \nabla_w logp(w|t, \mu)|_{w_{MP}} = -(\varphi^T|B\varphi + \mu)$$

$$\varphi = [\varphi(x_1), \varphi(x_2), .., \varphi(x_N)]^T \text{and B=diag } (\beta_1, \beta_2, .. \beta_n).$$

Make an application to complete the covariance. Update the hyperparameter after that. The relevance vector defines the model performance as a high-dimensional hyperplane that approximates the plane's test samples.

Experimental Results analysis: With a Python tool, the experimental analysis is carried out. Medical photographs from BRAINIX are stored in the database. The accuracy, precision, recall, and Peak Signal-to-Noise Ratio (PSNR) of the proposed LPDF-RVM technique are compared to Random Forest (RF) with GCNN.

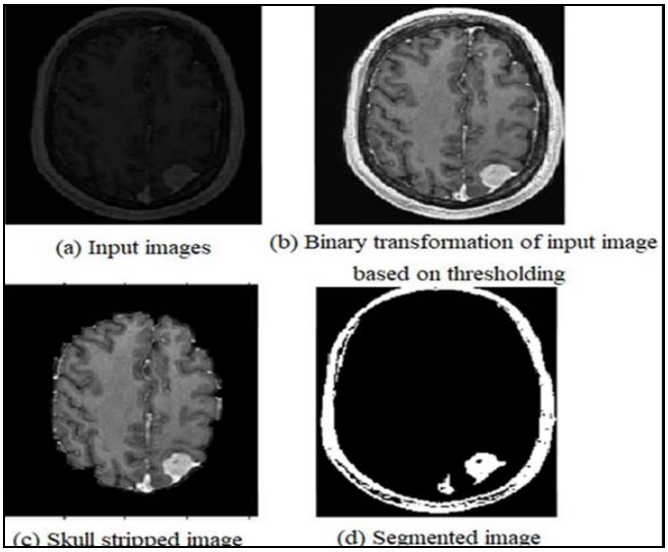

Fig 2: Segmentation Results

Fig.-2 shows the result of the method that was described. The Brain MRIs are first used as input. The binary transformation of the input image based on thresholding is displayed in Fig-2. The image of the skull stripping is shown in Fig.-2. Lastly, LPDF-RVM is used to obtain the segmented pictures, as illustrated in Fig.-3.

Table-1 presents an examination of the proposed LPDFRVM-GCNN model's performance using various metrics, including accuracy, precision, recall, and PSNR.

Table 1: Result analysis of existing method with proposed Lpdfrvm-Gcnn method

Measures	LSTM Model	CNN Model	RF-GCNN	LPDFRVM- GCNN
Precision	97.12	97.36	98.00	98.50
Recall	96.87	97.49	98.23	98.65
Accuracy	96.58	97.15	98.00	98.50
PSNR(dB)	90.97	93.22	96.64	97.00

Accuracy: Accuracy is an important measure that defines the overall efficiency of the model and is defined by

$$Accuracy = \frac{Tp + Tn}{(T_p + T_n + F_p + F_n)}$$

As shown in Fig-3, the accuracy performance of the suggested LPDF-RVM and GCNN scheme is compared with RF with GCNN. Plotting these methods follows the x-axis, while plotting accuracy follows the y-axis. Ultimately, it can be stated based on the results that the new LPDF-RVM performs better in terms of accuracy when compared to the current system.

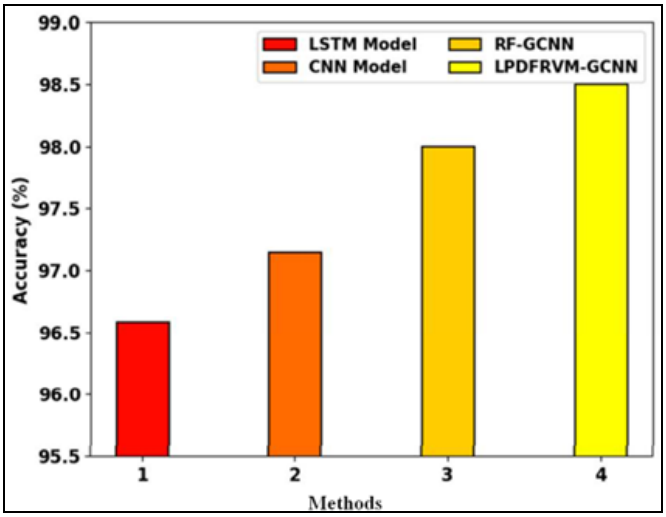

Fig 3: Accuracy comparison

Precision: Precision is determined by

$$Precison(P) = \frac{T_p}{T_p + F_p}$$

A comparison is made between the accuracy of the suggested LPDF-RVM and GCNN method and RF with GCNN. Plotting the models follows the x-axis, whereas plotting precision follows the y-axis. Fig-4 shows the level of precision achieved using various methods. Based on the statistics, it is evident that the model that was provided performed more effectively than the other technique indicated.

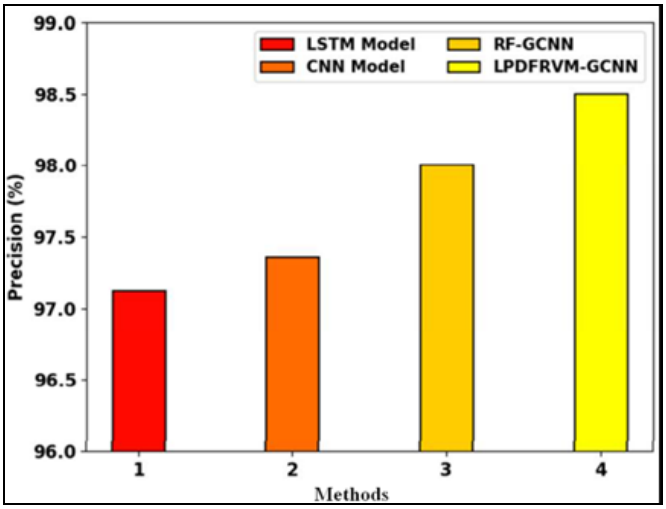

Fig 4: Precision comparison

Recall: The recall is ratio of correctly forecasted positive observations to every observation in actual class - yes. It can be calculated as:

$$Recall\ (R) = \frac{T_p}{T_p + F_n}$$

The recall performance of the suggested LPDF-RVM and GCNN scheme is compared with RF using the GCNN approach, as illustrated in Fig.-5. Plotting the current and future methods along the x-axis and recall along the y-axis respectively. The experimental results show that, as compared to previous strategies, the newly developed scheme achieves significantly higher recall.

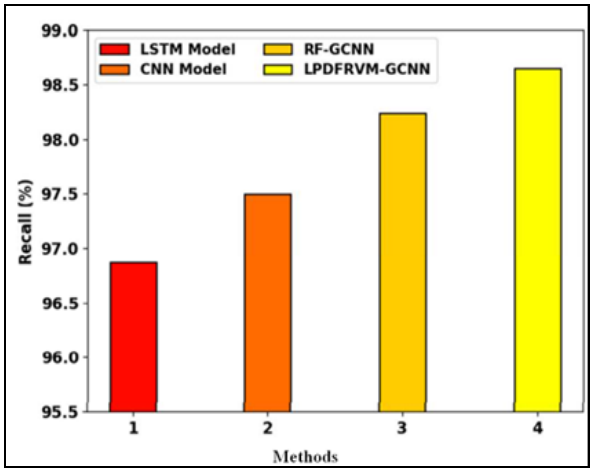

Fig 5: Recall comparison

PSNR comparison: The PSNR is used to measure the quality of the images. It is represented as:

$$PSNR = 10 \cdot \log_{10}\left(\frac{255^2}{MSE}\right)[dB]$$

In Fig.-6, the PSNRs of the suggested and current approaches are compared. Plotting the current and proposed methods is done along the x-axis, while the PSNR is plotted along the y-axis. The provided system achieves a greater PSNR value compared to the previous technique, based on the experimental results.

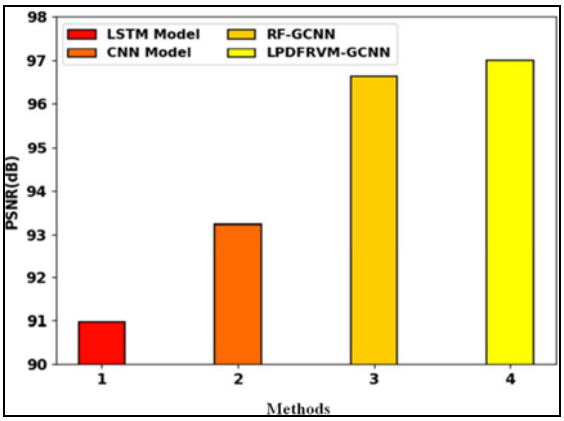

Fig 6: PSNR Comparison

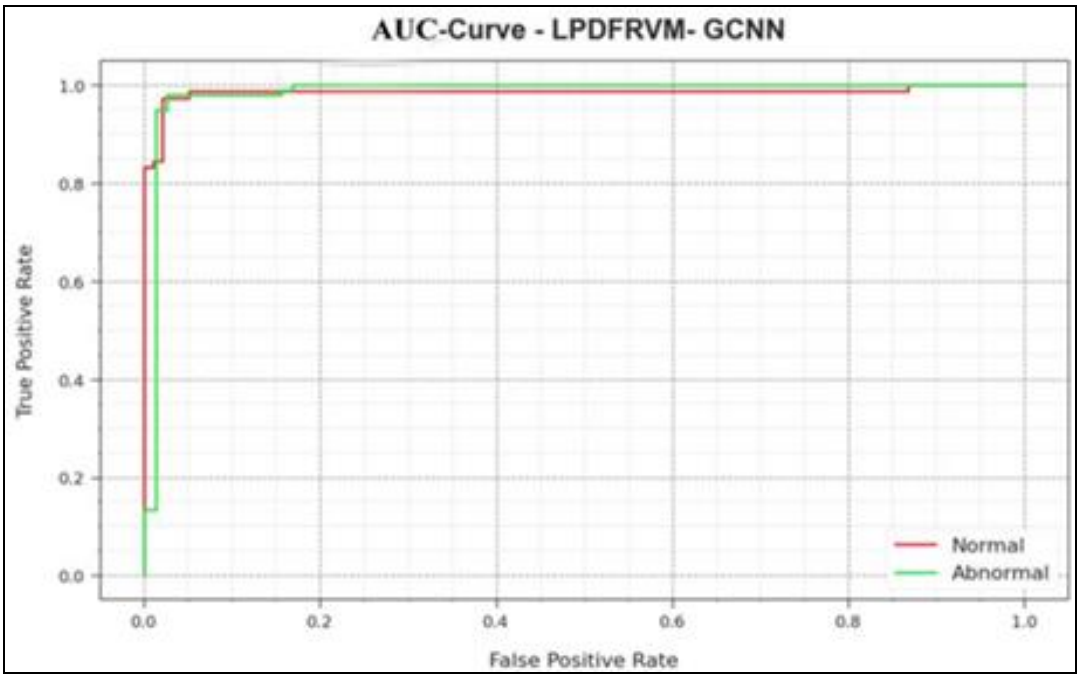

Fig 7: AUC Curve for LPDFRVM-GCNN Model

The LPDF-RVM model is used in the proposed LPDF-RVM and GCNN approach to segment the categorized tumor regions. The construction of the LPDF-RVM model for the segmentation process demonstrates the originality of the study, and the suggested model aids in identifying the tumor regions that are affected.

The system that was demonstrated used GCNN and LPDF-RVM to automatically segment BT data. WF is applied in order to reduce noise and enhance performance. After the skull stripping process is finished, GLCM and HOG feature extraction is carried out. For classification, GCNN is used based on the characteristics. Next, the segmentation process is carried out and divided into infected and non-infected portions using the LPDF-RVM. The experimental results show that the suggested approach performs as well as possible in comparison to earlier approaches in terms of accuracy, precision, recall, and PSNR.

Conclusion

We recognize the importance of further investigation and testing to thoroughly validate the effectiveness of our proposed method. The field of brain tumor identification in medical imaging remains a focal point of research, and our study utilizes five distinct convolutional models and transfer learning architectures to contribute to this area. Nevertheless, there remains ample opportunity for further exploration and advancement in this domain.

Continuous research into brain tumor detection systems has the potential to significantly enhance diagnostic accuracy for both patients and medical professionals in the challenging battle against brain cancers. By refining detection systems and pushing the boundaries of knowledge in this field, we aim to improve diagnostic capabilities and ultimately enhance patient outcomes. Additionally, conducting rigorous performance evaluations on a more comprehensive dataset will provide valuable insights into the model's ability to differentiate between various types of brain lesions. While our current dataset marks an initial step in brain tumor detection, future studies should aim to incorporate a more diverse and clinically relevant collection of brain lesions to address the complexities encountered in real-world diagnostic scenarios.

References

1. Alhassan AM, Wan Mohd Nazmee WH, Wan Zainon WA. BAT Algorithm with Fuzzy C-Ordered Means (BAFCOM) clustering segmentation and Enhanced Capsule Networks (ECN) for brain cancer MRI images classification. IEEE Access. 2020;8(3):2104-2122.
2. Aledhari M, Razzak R. An adaptive segmentation technique to detect brain tumors using 2D U-net. In: IEEE International Conference on Bioinformatics and Biomedicine (BIBM); c2020. p. 2328-2334.
3. Hirahara D. Preliminary assessment for the development of CAD system for brain tumor in MRI images utilizing transfer learning in Xception model. In: IEEE 8th Global Conference on Consumer Electronics (GCCE); c2019. p. 922-924.
4. Deepa R, Sam Emmanuel WR. MRI brain tumor classification using cuckoo search support vector machines and particle swarm optimization based feature selection. In: 2nd International Conference on Trends in Electronics and Informatics (ICOEI); c2018. p. 1213-1216.
5. Han Y, Zhang Z. Notice of violation of IEEE publication principles: Deep learning assisted image interactive framework for brain image segmentation. IEEE Access. 2020;8(11):117028-117035.
6. Karnan M, Gopal NN. Hybrid markov random field with parallel ant colony optimization and fuzzy c means for MRI brain image segmentation. In: IEEE International Conference on Computational Intelligence and Computing Research; c2010. p. 1-4.
7. Mallick PK, Ryu SH, Satapathy SK, Mishra S, Nguyen GN, Tiwari P. Brain MRI image classification for cancer detection using deep wavelet autoencoder-based

deep neural network. IEEE Access. 2019;7(2):46278-46286.
8. Jain M, Singh V, Rani A. A novel nature-inspired algorithm for optimization: Squirrel search algorithm. Swarm Evol Comput. 2019;44(2):148-175.
9. Mzoughi H, Njeh I, Slima MB, Benhamida A. Glioblastomas brain tumor segmentation using optimized U-Net based on Deep Fully Convolutional Networks (D-FCNs). In: 5th International Conference on Advanced Technologies for Signal and Image Processing (ATSIP); 2020. pp. 1-6.
10. Ronneberger O, Fischer P, Brox T. U-Net: Convolutional networks for biomedical image segmentation. In: International Conference on Medical Image Computing and Computer-Assisted Intervention. Springer; c2015. p. 234-241.
11. Sultan HH, Salem NM, Al-Atabany W. Multi-classification of brain tumor images using deep neural network. IEEE Access. 2019;7(21):69215-69225.
12. Xu Y, Jia Z, Ai Y, Zhang F, Lai M, Chang EI. Deep convolutional activation features for large scale brain tumor histopathology image classification and segmentation. In: IEEE International Conference on Acoustics, Speech and Signal Processing (ICASSP); c2015. p. 947-951.
13. Zhou C, Ding C, Wang X, Lu Z, Tao D. One-pass multi-task networks with cross-task guided attention for brain tumor segmentation. IEEE Trans Image Process. 2020;29(5):4516-4529.